www.nature.com/scientificreports

SCIENTIFIC REPORTS
natureresearch

OPEN

Ultrastructural analysis of SARS-CoV-2 interactions with the host cell via high resolution scanning electron microscopy

Lucio Ayres Caldas[1,5,6]✉, **Fabiana Avila Carneiro**[6], **Luiza Mendonça Higa**[2], **Fábio Luiz Monteiro**[2], **Gustavo Peixoto da Silva**[3], **Luciana Jesus da Costa**[3], **Edison Luiz Durigon**[4], **Amilcar Tanuri**[2] & **Wanderley de Souza**[1,5]

SARS-CoV-2 is the cause of the ongoing COVID-19 pandemic. Here, we investigated the interaction of this new coronavirus with Vero cells using high resolution scanning electron microscopy. Surface morphology, the interior of infected cells and the distribution of viral particles in both environments were observed 2 and 48 h after infection. We showed areas of viral processing, details of vacuole contents, and viral interactions with the cell surface. Intercellular connections were also approached, and viral particles were adhered to these extensions suggesting direct cell-to-cell transmission of SARS-CoV-2.

COVID-19 is an acute respiratory illness caused by the SARS-CoV-2—a novel coronavirus identified during this pandemic[1]. The outbreak started at Wuhan in Hubei province, China, in December 2019[2]. Since then, the world has seen a rapid spread of the virus with an increasing number of infected people—around 6 million cases and close to 400,000 deaths[3]. In the first four months, the outbreak has led to more than 28,000 deaths in Brazil[4]. There is currently no vaccine or specific treatment for COVID-19. Patients attendance is mainly based on supportive and symptomatic care. Therefore, a treatment capable of inhibiting viral infection and/or replication is urgent.

SARS-CoV-2 is an enveloped, positive-sense RNA beta-Coronavirus belonging to the *Coronaviridae* family. The genome is packaged inside a helix capsid formed by the nucleocapsid protein (N). Three other structural proteins are associated with the viral envelope: membrane (M), envelope (E), and glycoprotein spike (S). Cellular entry of SARS-CoV-2 depends on the binding of the S protein to angiotensin converting enzyme 2 (ACE2)—a specific cellular receptor located on the surface of the host cell[5,6]. This is a common receptor for SARS-CoV as well[7,8] (Li et al., 2003; 2005); this receptor facilitates zoonotic transfer because these viruses can engage ACE2 from different animal species[9].

Beta-coronaviruses replicate in the cytoplasm; cellular compartments like the endoplasmic reticulum (ER) and the endoplasmic reticulum-Golgi apparatus intermediate compartiment (ERGIC) go through intense remodeling. This implies the contribution of host membranes and organelles for viral replication. Therefore, remodeling of intracellular membranes due to coronavirus infection is also observed for many RNA viruses[10].

[1]Laboratório de Ultraestrutura Celular Hertha Meyer, Instituto de Biofísica Carlos Chagas Filho, Cidade Universitária. Av., Carlos Chagas Filho 373, Prédio CCS, Bloco C, subsolo, CEP: 21941902, Rio de Janeiro, RJ, Brazil. [2]Departamento de Genética, Instituto de Biologia, Universidade Federal Do Rio de Janeiro, Rio de Janeiro, Brazil. [3]Departamento de Virologia, Instituto de Microbiologia Paulo de Góes, Universidade Federal Do Rio de Janeiro, Rio de Janeiro, Brazil. [4]Instituto de Ciências Biomédicas, Universidade de São Paulo, São Paulo, Brazil. [5]Instituto Nacional de Ciência e Tecnologia de Biologia Estrutural e Bioimagem, Rio de Janeiro, Brazil. [6]Present address: Núcleo Multidisciplinar de Pesquisa UFRJ-Xerém em Biologia – NUMPEX-BIO, Universidade Federal Do Rio de Janeiro, Campus Duque de Caxias Geraldo Cidade. CEP: 25265-970, Rio de Janeiro, RJ, Brazil. ✉email: lucio@biof.ufrj.br

After internalization and RNA release into the cytoplasm, a set of proteins is synthesized triggering the formation of vesicles that become a viral platform ensuring efficient replication and transcription of the RNA[11,12].

New coronavirus particles are assembled in the endoplasmic reticulum and Golgi complex. Membrane budding between these compartments was reported in association with N protein and genomic RNA along with M, E, and S proteins. The complete virions are delivered to the extracellular environment following a conventional secretory route[13–15].

The research community has sought to better understand the genetic makeup of the virus and thus discover how to effectively treat it. Social isolation for 14 days is the main way to prevent the disease from spreading. Quarantine and lockdowns were implemented in cities with high rates of infection and mortality[3]. Death is common in patients with severe symptoms including shortness of breathing, fever, lethargy, respiratory failure, and/or thrombosis[16,17].

Understanding the virus-cell interactions is key to vaccines, treatments, and diagnoses. Most microscopic studies of SARS-CoV-2 were performed with transmission electron microscopy. Here, we used high resolution scanning electron microscopy (SEM) to study inner cellular structures. The results offer evidence of infection-induced cellular remodeling and the formation of a specialized region for viral morphogenesis. We also show intercellular extensions for viral cell surfing. These observations offer new insights into the transmission of SARS-CoV-2.

Material and methods

Cells and virus. SARS-CoV-2 isolate (HIAE-02: SARS-CoV-2/SP02/human/2020/BRA (GenBank accession number MT126808.1) was used in this work. The virus was grown in Vero cells (Monkey African Green kidney cell line – ATCC CCL-81) in the Laboratory of Molecular Virology, at Federal University of Rio de Janeiro, Brazil. Vero cells were maintained in DMEM supplemented with 5% fetal bovine serum (FBS; GIBCO) at 37 °C and 5% CO_2. All work involving infectious SARS-CoV2 was performed in a biosafety level (BSL)-3 containment laboratory.

Infection assays. Semi-confluent (70%) cells were grown on sterile glass coverslips in 24-well tissue culture plates infected with MOI (multiplicity of infection – the rate of virus per cell) values of 0.01, 0.1, or 1 using SARS-CoV-2 in free-serum medium. Fresh medium containing 5% FBS was added after an absorption period of 1.5 h at 37 °C and 5% CO_2. Cells were processed for electron microscopy 2 or 48 h post-infection (hpi).

High resolution scanning electron microscopy. After 2 or 48 h post-infection (hpi), samples were fixed with 2.5% glutaraldehyde in 0.1 M cacodylate buffer (pH 7.2) for 2 h. The coverslips were washed with 0.1 M sodium cacodylate buffer and post-fixed for 40 min in 1% OsO_4 with 0.8% potassium ferrocyanide. After another washing cycle, the samples were dehydrated through a series of increasing concentration (30%–100%) of ethanol. The samples were critical-point-dried in liquid CO_2 in a BALZERS CPD apparatus before monolayer scraping with a conventional adhesive SCOTCH tape as in previous studies[18]. This technique does not totally remove the plasma membrane, as happens when detergent extraction is used, but provides the exposing of large areas of the inner portion of the cells. They were then sputtered with a 5-nm thick platinum coat in a BALZERS apparatus. Samples were observed using an Auriga ZEISS microscope operated between 1.0 and 1.8 kV.

Results

To identify alterations on the surface of SARS-CoV-2-infected cells, we compared their morphology and the occurrence of surface projections (SP). While we did not detect any significant alteration in cell shape, the presence of SP increased on the surface of infected cells at 2 hpi (Fig. 1A–C). However, no viral particles were observed adhering to the cell surface or beneath these projections (Fig. 1D). At 48 hpi, we compared the surfaces of mock and infected cells (MOI of 0.1) to highlight the presence of viral particles adhered to the smooth cell surface and to the SP (Fig. 1E, F).

At the same time, and with a MOI of 1, viruses that egressed from a previous cycle of infection were observed during the process of attachment to the cell plasma membrane (Fig. 2A). The corona-like features of the SARS-CoV-2 particles were discernible via SEM (Fig. 2B), and the measurements showed sizes of approximately 80 nm in diameter (Fig. 2C).

Removal of the host cell plasma membrane before platinum sputtering exposed the interior of the mock and infected cells. While mock cells displayed a diffuse distribution of organelles (Fig. 2D), infected cells exhibited a more polarized disposition of organelles and pit-coated vesicles approximately 100 nm in diameter (Fig. 2E, F). With a MOI of 1, cells at 48 hpi showed a plethora of vacuoles (0.4 to 1 µm; Fig. 3A). These were translocated to the cell plasma membrane presumably to perform exocytosis of viral particles (Fig. 3B). Some of these vacuoles had their content revealed and were filled with immature viruses, amorphous materials, or a hemocyte-like format (Fig. 3C–E). Although no virus-like particles could be distinguished in the ER, bordering vesicles were observed on the vacuoles (Fig. 3D).

Cells at 48 hpi also had viral particles near the cell surface membrane ruffles (Fig. 4A) and a filopodium-like structure (Fig. 4B). Other viral particles were wrapped with thin (≃ 70 nm) cellular projections that resemble nanotubes (Fig. 4C). Membrane bridges that connect two cells showed the presence of virus particles on their surface (Figs. 4D,E).

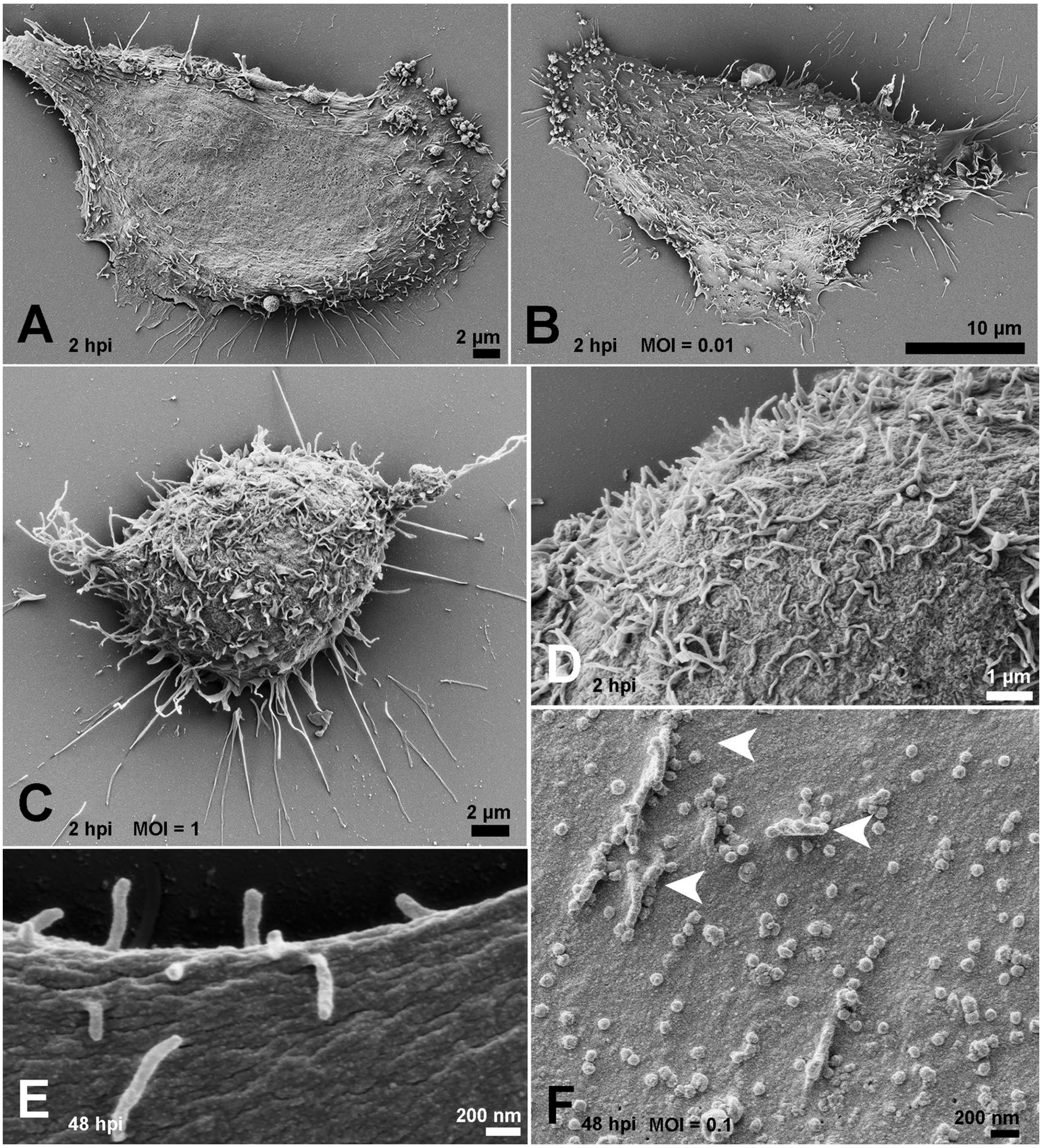

Figure 1. Effect of SARS-CoV-2 infection on host cell surface at 2 and 48 hpi. At 2hpi, mock-infected cells exhibited smooth surfaces (**A**), while infected cells presented a discreet increment in the number of SP with the MOIs of 0.01 (**B**) and 1 (**C**). No viral particles were observed on the surface of infected cells at 2hpi, even with the MOI of 1 (**D**). (**E**) Mock-infected cell surface at 48 h. (**F**) Virus adhesion to the cell surface and SP (arrowheads) became more evident with the MOI of 0.1 (**F**). Bars: (**A**, **C**) 2 µm; (**B**) 10 µm; (**D**) 1 µm; (**E**, **F**) 200 nm.

Discussion

Part of the challenge in controlling COVID-19 is the innovative features of this coronavirus. New knowledge on virus genetics and morphology needs to be analyzed concurrently with viral "behavior" within the host cell as well as the dynamics that determine the fate of the particle. To approach SARS-CoV-2/cell interactions, we investigate several steps of virus infection in Vero cells at 2 and 48 hpi by SEM. Vero cells are a widely used model used in viral infection studies and is an adequately supports coronavirus replication[12,14,15,19]. This microscopic approach detailed virus-induced changes in the cell.

Our assays were performed using three MOIs (0.01; 0.1 and 1), and we could discern the MOI of 0.1 as the more adequate for this type of study. This MOI allowed the best cell conditions and distribution and also allowed visualization of virions through the cell surface into the cell interior.

The absence of virions adhered to the cells surface at 2 hpi corroborates recent studies performed by Belhaouari et al.[19] in which SARS-CoV-2 particles were only observed at these loci after 12 hpi. In contrast,

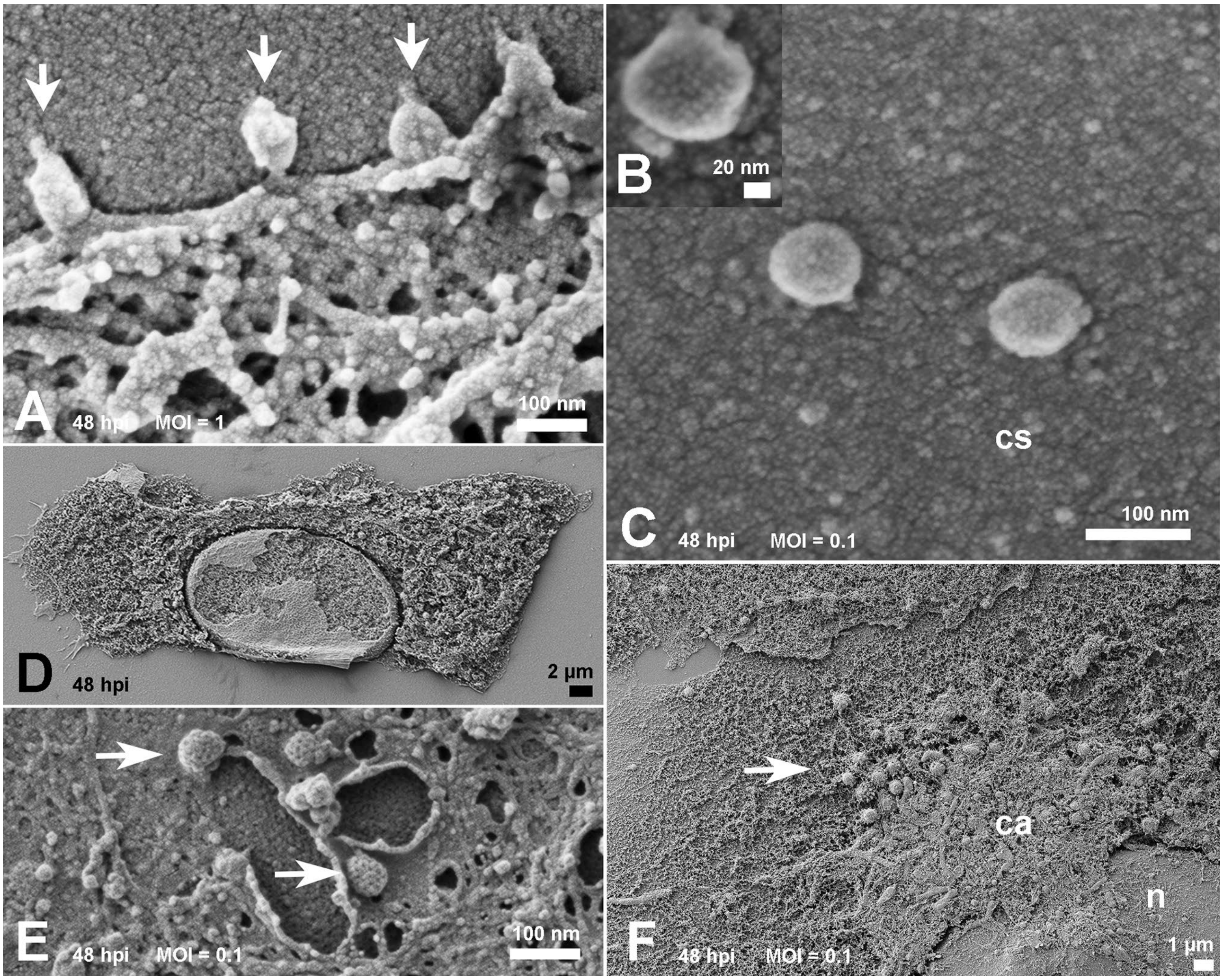

Figure 2. Morphology of cells surface and interior at 48 hpi. (**A**) With the MOI of 1, virus attachment (arrows) was frequent. (**B**) Spikes of SARS-CoV-2 particles observed on the cell surface were discernible (MOI of 0.1). Viruses observed on cell surface (cs) exhibited a size between 70 and 85 nm (**B**, **C**) at MOIs of 0.01 and 0.1 respectively. Scraping of cells plasma membrane (**D**) revealed a homogeneous distribution of organelles in mock-infected samples, Infected cells exhibited coated pits vesicles of ≃ 100 nm (arrows) at perinuclear sites (**E**). A polarized disposal at the infected cells cytosol (**F**) represented as a condensed area (ca) in the infected ones (MOI of 0.1). (n): nucleus; Bars: (**A**, **C**, **E**) 100 nm; (**B**) 20 nm; (**D**) 2 µm; (**F**) 1 µm.

SARS-CoV-2 particles were found lying on the cellular surface at 48 hpi between surface projections and adhered to them. We also observed probable viral particles inside vacuoles suggesting a secretion route. These aggregates of cell organelles and components (Fig. 2F) may reflect the polarized release of virus previously described for SARS-CoV[20].

All viruses measured by SEM display a spiky round shape with a size of around 70–85 nm in diameter considering a platinum coating of 5 nm. This agrees with the dimensions described in recent studies[1,21,22].

Viral particles adhered to smooth surface and microvilli-like surface projetions. The effects on the surface morphology of infected cells varies among viruses. Infection by several viruses including HTLV-IIIB leads to a loss of cell SP that are then replaced by blebs[23]. Microvilli induction or increases were reported in several cases of DNA or RNA viral infection[24,25]. For RNA viruses that egress by budding, e.g., influenza, the increase in SP of infected cells coincides with higher budding rates[26].

Similar to prior studies on SARS-CoV infection of Vero cells[27], we also observed a ruffled host cell and thickened edges displaying a layered shape. These sites were appropriate to register the attachment of SARS-CoV-2 particles (Fig. 2A) similar to transmission electron microscopy images of the same early step of SARS-CoV infection of Vero cells[28].

Likewise, the proliferation of SP on the infected cells, especially at the apical region of these cells, is similar to SARS-CoV and SARS-CoV-2. In addition, the abundance of SARS-CoV-2 particles held on SP, was recently showed[29] and may facilitate the speed of viral propagation in the epithelium of conducting airways from the lumen of the respiratory superior tract because this environment is colonized by ciliated cells.

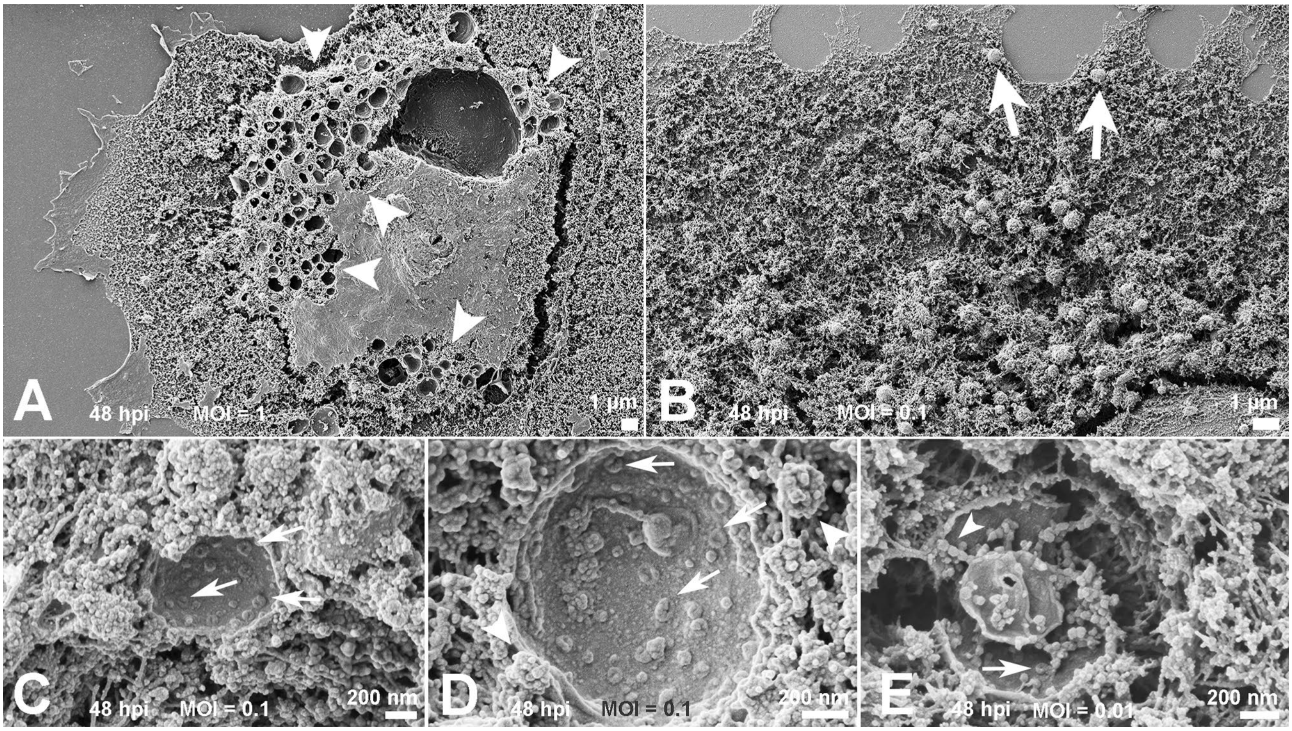

Figure 3. Inspection of the condensed areas of cells at 48 hpi. (**A**) Profusion of vacuoles (arrowheads) in cells infected with the MOI of 1. The possible route of the vacuoles was indicated by arrows in (**B**). Scraped vacuoles had at least part of their content exposed. Vacuoles in (**C**) and (**D**) presented doughnut-like particles (arrows). In (**D**), borderinng vesicles (arrowheads) could be recognized next the vacuole membrane. Vacuoles shown in (**E**) display doughnut-like particles (arrow) and immature viral-like particles (arrowhead) too. MOIs: (**B**–**D**) 0.1; (**E**) 0.01; Bars: (**A**, **B**) 1 µm; (**C**–**E**) 200 nm.

Vacuoles containing viral particles.

Cell scraping is a very useful expedient that is occasionally used in studies of host cell/parasite interactions[30,31]. Infected cells are artificially devoid of plasma membranes and exposed to a myriad of vacuoles (Fig. 3A). Drastic vacuolization due to viral infection was previously described for other RNA viruses including SARS-CoV[20,32]. Similar sites were recently reported as virus morphogenesis matrix vesicae (VMMV)[19]. The particles observed in the interior of these VMMVs (Fig. 3C-E) were previously described as doughnut-like particles when observed by electron microscopy[19,33]. SARS-CoV immature particles are presumed to bud into vesicles as part of the assembly process, and thus the observed particles were probably immature viruses devoid of the representative (corona) spikes of this virion. Bordering vesicles were found in close association with the vacuoles (Fig. 3D), and thus we speculate that their role in viral pre-components leads to discharge into the compartments.

Studies with other coronaviruses identified large virion-containing vacuoles (LVCVs) where the complete particle would bud. There is correlation between these structures as observed by transmission electron microscopy and our data suggesting the occurrence of both phenomena.

Translocation of vacuoles towards the plasma membrane.

Coronaviruses infection leads to massive remodeling of cell membranes[34,35]; the more condensed area depicted in the cytoplasm at 48 hpi (Fig. 2F) may correspond to the main locus of viral morphogenesis. The proposed mechanism for the export of viruses to the extracellular space is via fusion of the transport compartment membrane with the cell plasma membrane[20].

The size of the vacuoles we observed in the cell periphery was not compatible with the identified clathrin-coated pits because the vacuoles measure approximately 1 µm; clathrin-coated pits measure near 200 nm in diameter. The presence of these endocytosis-associated players was recently reported in SARS-CoV-2-infected cells. They are likely receptacles to the nucleocapsid after the incoming virus is uncoated[19].

Thus, our observations suggest that a boost in vacuoles is restricted only to a specific and more condensed part of the cytoplasm. This suggests translocation to the plasma membrane is required for release the viral particles by a fusion mechanism.

Cellular bridges containing viral particles.

Viral particles adhered to cell surface protrusions that were shown to connect two cells. This observation suggests viral "cell surfing" previously described by other enveloped viruses such as HIV and human metapneumovirus[36,37]. This mechanism is presumed to allow the in vivo penetration of virus in mucosal surfaces that display microvilli-rich cells.

Actin filaments play a fundamental role in viral extrusion by the cell for both RNA and DNA viruses. Actin offers the strength to discharge the progeny virus particles to the extracellular medium, as occurs to some viruses

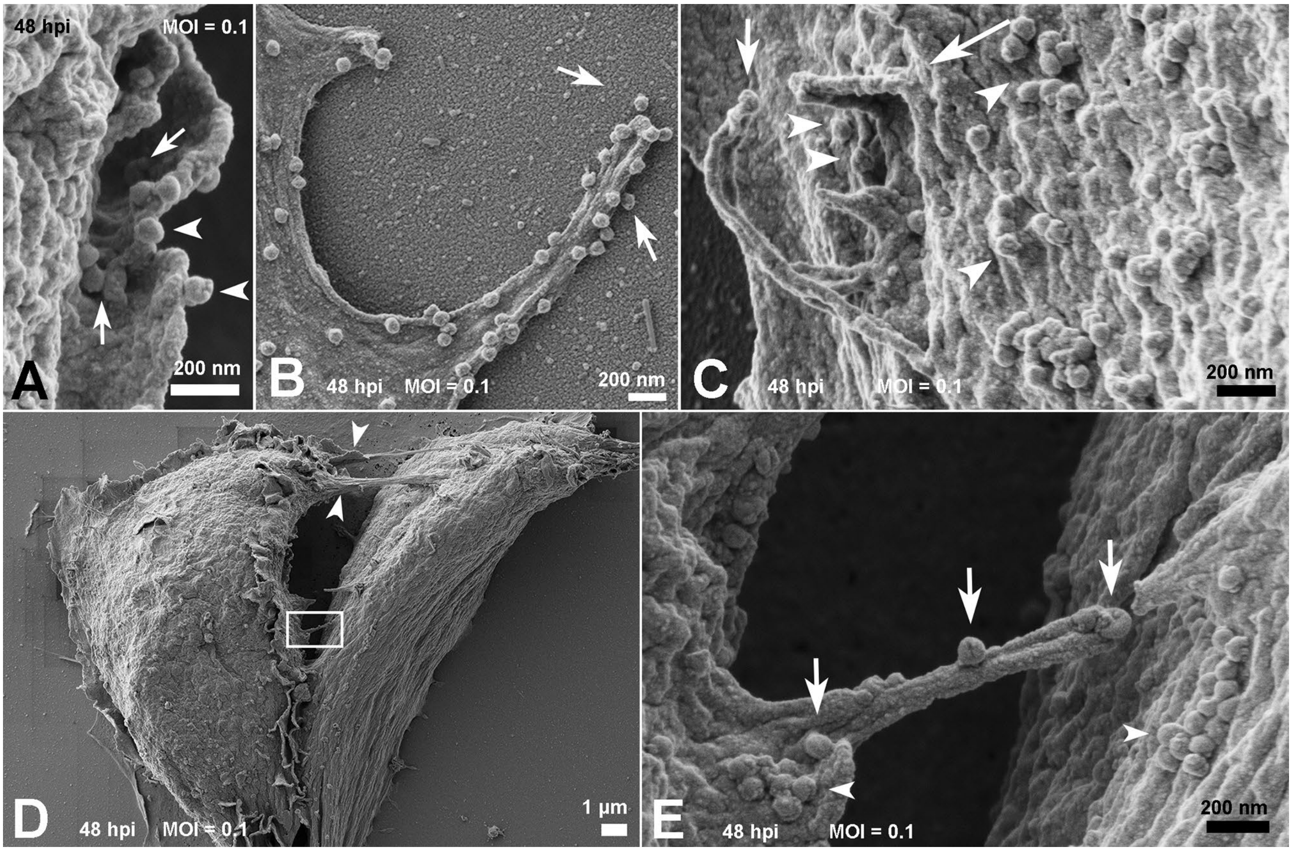

Figure 4. Fate of the SARS-CoV-2 particles adhered to the cell surface at 48 hpi. (**A**, **B**) Cell membrane ruffles about to wrap several viral particles (arrows). Viruses could also be observed on the edge of membrane ruffles (arrowheads) (**A**) and phyllopodium-like extensions (**B**). In (**C**) a viral particle could be seen adhered to the edge of the microvilli-like structure (arrow) next to membrane ruffles (long arrow) surrounding SARS-CoV-2 particles (arrowheads). (**D**) Communications between two infected cells are indicated with arrowheads. One of the bridges between the cells was depicted in the rectangle. A higher magnification of this area is shown in (**E**) and displays viral particles (arrows) on their surface. Aggregates of SARS-CoV-2 particles (arrowheads) were also observed on the surface of both cells. MOI = 0.1; Bars: (**A**–**C**, **E**) 200 nm; (**D**) 1 µm.

that leave the cell by budding, including Fowlpox and West Nile viruses[38,39]. Other examples include actin comets—these are an efficient form of poxvirus dissemination and cell-to-cell HIV spreading, which involves the direct engagement of GAG proteins and F-actin[40,41].

Previous studies have shown that the cytoskeleton network plays an important role in the maturation and, possibly, in the replication process of SARS-CoV[27]. Communication between the two cells in Fig. 4C-D suggests the occurrence of a thin (< 0.7 µm) strand of F-actin containing tunneling nanotube (TNT). These intercellular membranous connections may provide the transference of molecular information especially viruses[42]. Similarly, virus cell surfing was shown on SARS-CoV-2 infection, which offers new insights into cell-to-cell propagation and virus transmission.

Received: 10 June 2020; Accepted: 24 August 2020
Published online: 30 September 2020

References

1. Zhu, N. *et al.* A novel coronavirus from patients with pneumonia in China, 2019. *N. Engl. J. Med.* **382**, 727–733 (2020).
2. Wu, F. *et al.* A new coronavirus associated with humanrespiratory disease in China. *Nature* **579**, 265–269 (2019).
3. World Health Organization. Coronavirus disease (COVID-19) pandemic https://www.who.int/emergencies/diseases/novel-coronavirus-2019 (2020).
4. Ministry of Health/Health Surveillance Secretariat. Special epidemiological bulletin COE-COVID-19. https://www.saude.gov.br/images/pdf/2020/May/21/2020-05-19---BEE16---Boletim-do-COE-13h.pdf (2020).
5. Walls, A. C. *et al.* Structure, function, and antigenicity of the SARS-CoV-2 spike glycoprotein. *Cell* **181**(2), 281-292.e6 (2020).
6. Zhou, P. *et al.* A pneumonia outbreak associated with a new coronavirus of probable bat origin. *Nature* **579**, 270–273 (2020).
7. Li, W. *et al.* Angiotensin-converting enzyme 2 is a functional receptor for the SARS coronavirus. *Nature* **426**, 450–454 (2003).
8. Li, F., Li, W., Farzan, M. & Harrison, S. C. Structure of SARS coronavirus spike receptor-binding domain complexed with receptor. *Science* **309**, 1864–1868 (2005).
9. Li, F. Structural analysis of major species barriers between humans and palm civets for severe acute respiratory syndrome coronavirus infections. *J. Virol.* **82**(14), 6984–6991 (2008).
10. Fehr, A. R. & Perlman, S. Coronaviruses: an overview of their replication and pathogenesis. *Methods Mol. Biol.* **1282**, 1–23 (2015).

11. Novoa, R. R. *et al.* Virus factories: associations of cell organelles for viral replication and morphogenesis. *Biol. Cell.* **97**, 147–172 (2005).
12. Miller, S. & Krijnse-Locker, J. Modification of intracellular membrane structures for virus replication. *Nat. Rev. Microbiol.* **6**, 363–374 (2008).
13. De Haan, C. A. & Rottier, P. J. Molecular interactions in the assembly of coronaviruses. *Adv. Virus Res.* **64**, 165–230 (2005).
14. Knoops, K. *et al.* SARS-coronavirus replication is supported by a reticulovesicular network of modified endoplasmic reticulum. *PLoS Biol.* **6**, e226 (2008).
15. Perlman, S. & Netland, J. Coronaviruses post-SARS: update on replication and pathogenesis. *Nat. Rev. Microbiol.* **7**, 439–450 (2009).
16. Rey, J.R. *et al.* COVID-19 and simultaneous thrombosis of two coronary arteries. *Rev. Esp. Cardiol.* Preprint at https://www.revespcardiol.org/en-covid-19-simultaneous-thrombosis-two-coronary-avance-S1885585720302565 (2020).
17. Udugama, B. *et al.* Diagnosing COVID-19: the disease and tools for detection. *ACS Nano* **14**(4), 3822–3835 (2020).
18. Caldas, L. A., Azevedo, R. C., da Silva, J. L. & de Souza, W. Microscopy analysis of Zika virus morphogenesis in mammalian cells. *Sci. Rep.* **10**(1), 8370 (2020).
19. Belhaouari, D.M. *et al.* The strengths of scanning electron microscopy in deciphering SARS-CoV-2 infectious cycle. *IHU Méditerranée Infection*. Ahead of print (2020).
20. Sims, A. C., Burkett, S. E., Yount, B. & Pickles, R. J. SARS-CoV replication and pathogenesis in an in vitro model of the human conducting airway epithelium. *Virus Res.* **133**(1), 33–44 (2008).
21. Kim, J.-M. *et al.* Identification of coronavirus isolated from a patient in Korea with COVID-19. *Osong Public Health Res. Perspect.* **11**, 3–7 (2020).
22. Prasad, S. *et al.* Transmission electron microscopy imaging of SARS-CoV-2. *Indian J. Med. Res.* **151**(2 & 3), 241–243 (2020).
23. Hockley, D. J., Wood, R. D., Jacobs, J. P. & Garrett, A. J. Electron microscopy of human immunodeficiency virus. *J. Gen. Virol.* **69**(Pt 10), 2455–2469 (1988).
24. Krempien, U., Jockusch, B. M. & Jungwirth, C. Herpes simplex virus-induced cell surface protrusions. *Intervirology* **22**(3), 156–163 (1984).
25. Wolffe, E. J., Weisberg, A. S. & Moss, B. Role for the Vaccinia virus A36R outer envelope protein in the formation of virus-tipped actin-containing microvilli and cell-to-cell virus spread. *Virology* **244**(1), 20–26 (1998).
26. Kolesnikova, L. *et al.* Influenza virus budding from the tips of cellular microvilli in differentiated human airway epithelial cells. *J. Gen. Virol.* **94**(Pt 5), 971–976 (2013).
27. Ng, M. L. *et al.* Topographic changes in SARS coronavirus–infected cells during late stages of infection. *Emerg. Infect. Dis.* **10**(11), 1907–1914 (2004).
28. Ng, M. L., Tan, S. H., See, E. E., Ooi, E. E. & Ling, A. E. Early events of SARS coronavirus infection in Vero cells. *J. Med. Virol.* **71**(3), 323–331 (2003).
29. Bouhaddou, M. *et al.* The global phosphorylation landscape of SARS-CoV-2 infection. *Cell* **182**, 1–28 (2020).
30. Caldas, L. A., Attias, M. & de Souza, W. A structural analysis of the natural egress of *Toxoplasma gondii*. *Microbes Infect.* **20**(1), 57–62 (2018).
31. De Souza, W. & Attias, M. New advances in scanning microscopy and its application to study parasitic protozoa. *Exp. Parasitol.* PMID: 29702111 Review (2018).
32. Caldas, L. A., Freitas, T. R. P., Azevedo, R. C. & de Souza, W. Prostaglandin A_1 inhibits the replication of bovine viral diarrhea virus. *Braz. J. Microbiol.* **49**(4), 785–789 (2018).
33. Qinfen, Z. *et al.* The life cycle of SARS coronavirus in Vero E6 cells. *J. Med. Virol.* **73**, 332–329 (2004).
34. Ulasli, M., Verheije, M. H., de Haan, C. A. & Reggiori, F. Qualitative and quantitative ultrastructural analysis of the membrane rearrangements induced by coronavirus. *Cell Microbiol.* **12**, 844–861 (2010).
35. Zhou, X. *et al.* Ultrastructural characterization of membrane rearrangements induced by Porcine Epidemic Diarrhea Virus infection. *Viruses.* **9**(9), 251 (2017).
36. Lehmann, M. J., Sherer, N. M., Marks, C. B., Pypaert, M. & Mothes, W. Actin- and myosin-driven movement of viruses along filopodia precedes their entry into cells. *J Cell Biol* **170**, 317–325 (2005).
37. El Najjar, F. *et al.* Human Metapneumovirus induces reorganization of the actin cytoskeleton for direct cell-to-cell spread. *PLoS Pathog.* **12**(9), e1005922 (2016).
38. Boulanger, D., Smith, T. & Skinner, M. A. Morphogenesis and release of fowlpox virus. *J. Gen. Virol.* **81**, 675–687 (2000).
39. Chu, J. J. H., Choo, B. G. H., Lee, J. W. M. & Ng, M. L. Actin filaments participate in West Nile (Sarafend) virus maturation process. *J. Med. Virol.* **71**, 463–472 (2003).
40. Carlson, L. A. *et al.* Cryo electron tomography of native HIV-1 budding sites. *PLoS Pathog.* **6**, e1001173 (2010).
41. Stradal, T. E. B. & Schelhaas, M. Actin dynamics in host-pathogen interaction. *FEBS Lett.* **592**(22), 3658–3669 (2018).
42. Jansens, R. J. J., Tishchenko, A. & Favoreel, H. W. Bridging the gap: virus long-distance spread via tunneling nanotubes. *J. Virol.* **94**(8), e02120-e2219 (2020).

Acknowledgements

We thank Professor Kildare Miranda (CENABIO) for providing the microscopy facilities; Dr. Lorian Cobra Straker (CENABIO) and Flávio Augusto Ferreira Martins Bezerra (INMETRO) for technical assistance. This work has been supported by Fundação Carlos Chagas Filho de Amparo à Pesquisa do Estado do Rio de Janeiro-FAPERJ, Financiadora de Estudos e Projetos-FINEP and Conselho Nacional de Desenvolvimento Científico e Tecnológico-CNPq.

Author contributions

Isolate preparations and virus growth were conducted by G.P.S. and L.J.C. Infections were performed by L.M.H. and F.L.M. Sample preparations and microscopy analysis were performed by L.A.C. and F.A.C.; analysis of the results was performed by L.A.C., F.A.C. and W.S. W.S. and A.T. contributed to the initial conception and design of this work. The first draft of the manuscript was written by L.A.C. and F.A.C. L.J.C., A.T. and W.S. commented on previous versions of the manuscript. E.L.D. provided SARS-CoV-2 isolate. All the authors were involved in reviewing and editing the manuscript. All authors read and approved the final manuscript.

Competing interests

The authors declare no competing interests.

Additional information

Correspondence and requests for materials should be addressed to L.A.C.

Reprints and permissions information is available at www.nature.com/reprints.

Publisher's note Springer Nature remains neutral with regard to jurisdictional claims in published maps and institutional affiliations.

Open Access This article is licensed under a Creative Commons Attribution 4.0 International License, which permits use, sharing, adaptation, distribution and reproduction in any medium or format, as long as you give appropriate credit to the original author(s) and the source, provide a link to the Creative Commons licence, and indicate if changes were made. The images or other third party material in this article are included in the article's Creative Commons licence, unless indicated otherwise in a credit line to the material. If material is not included in the article's Creative Commons licence and your intended use is not permitted by statutory regulation or exceeds the permitted use, you will need to obtain permission directly from the copyright holder. To view a copy of this licence, visit http://creativecommons.org/licenses/by/4.0/.

© The Author(s) 2020